

**The Sun & the Heliosphere
as an Integrated System**

Chairpersons: G. Poletto and S.T. Suess

Editors: G. Poletto (Chief-Editor) and S.T. Suess

JD 7: The Sun and the Heliosphere as an Integrated System

Giannina Poletto

*INAF - Arcetri Astrophysical Observatory, Largo Fermi, 5, 50125
Firenze, Italy*

Steven T. Suess

NASA-MSFC, MS SD50, Huntsville, AL 35812, USA

Abstract. We summarize here the oral contributions given at the Joint Discussion (JD) 7 *The Sun and the Heliosphere as an Integrated System*, held on July 17, 2003, in Sydney, as part of IAU XXV and give a list of posters presented at the JD.

1. Introduction

As knowledge of the Sun and the heliosphere grows, it is becoming not only possible but preferable to view the global structure, the interaction with the local interstellar medium, and changes over a solar cycle as the behavior of an integrated system. This consideration motivated Joint Discussion 7, which was meant both to summarize the state of art at the time of IAU XXV and to solicit interest in this kind of approach. The Joint Discussion was arranged in four sections, two on processes that, beginning from the Sun's interior, model and shape the heliosphere (*From the Transition Region to the Corona and Beyond* and *From the Sun to the Interstellar Medium*), one on elemental abundances and particles in the corona and the heliosphere (*Energetic Particles, Energetic Neutral Atoms and Composition*) and one on forthcoming solar and heliospheric space missions. In the following we give a brief summary of the contributions presented at the JD in each section. An extended discussion of the topics covered by JD is expected to appear in a comprehensive book on the Sun and the Heliosphere which will be edited by us and printed by Kluwer in year 2004. Posters which were exhibited as part of the Joint Discussion are listed at the end of this summary.

2. Program

2.1. Scientific Program

Session I: From the Sun to the Interstellar Medium

Chair: H. Cane

Ulysses at Solar Maximum: Selected Highlights

Hydrogen Walls: Mass Loss of Dwarf Stars and the Young Sun

Radio Emission from the Outer Heliosphere and Beyond
MHD Turbulence in the Heliosphere

Session II: From the Transition Region to the Corona and beyond

Chair: G. Poletto

The Magnetic Field from the Sun to the Interstellar Medium

The 3D Solar Wind over the Solar Cycle
Observed by IPS

Invited Speaker

R. Marsden

J. L. Linsky,

B. E. Wood,

and G. P. Zank

I. Cairns

B. Bavassano

The Chromosphere-Corona Coupling and the Solar Wind
The Bastille Day Event: from Solar Surface to the

Far Heliosphere

Session III: Energetic Particles, Energetic Neutral Atoms, and Composition

Chair: B. Fleck

Elemental Abundances in the Solar Corona

The Heliospheric Interface: Theory and Observations

Propagation of Energetic Particles to High Latitudes
Particles in the Heliosphere: An Overview

Invited Speaker

J. Raymond

V. Izmodenov

T. Sanderson

R. Wimmer
-Schweingruber

Session IV: New Missions

Chair: S. Suess

Novel Solar and Heliospheric Research with
Solar Orbiter

The International Living With a Star Program

Invited Speaker

E. Marsch

H. Opgenoorth,
M. Guhathakurta,
and R. Marsden

2.2. Scientific Organizing Committee

The SOC included: I. Cairns (Local Liaison, Australia), B. Fleck (The Netherlands), R. Forsyth (U.K.), G. Poletto (Co-Chair, Italy), H. Cane (Australia), R. Lallement (France), S. T. Suess (Co-Chair, U.S.A.), A. V. Usmanov (Russia), J. X. Wang (China), H. Washimi (Japan), T. Zurbuchen (U.S.A.).

3. From the Sun to the Interstellar Medium

3.1. Ulysses at Solar Maximum: Selected Highlights

The original objective of Ulysses was to “investigate for the first time as a function of heliographic latitude the properties of the solar wind, the structure of the Sun/wind interface, the heliospheric magnetic field, solar radio bursts and plasma waves, solar X-rays, solar and galactic cosmic rays, and both interstellar and interplanetary neutral gas and dust.” The 6.2 year orbit, inclined by 80 degrees to the heliographic equator, with an aphelion of 5.4 AU and perihelion of 1.34 AU, has allowed Ulysses to meet this original objective and go on to make fundamental contributions and discoveries related to the 3D heliosphere and also to the Sun, Jupiter, the local interstellar medium, the Milky Way, and the origins of gamma ray bursts. Orbit I was completed in 1998, covering solar sunspot minimum, and Orbit II is nearing completion. Orbit III will then provide coverage during the second half of the 22 year solar magnetic cycle. R. Marsden (European Space Agency, Noordwijk, The Netherlands) reviewed existing Ulysses’ results and what Ulysses will be doing over the coming 4 years.

Solar wind plasma measurements during Orbit II illustrate the difference between the simple bimodal structure at solar minimum and the variable flows seen at all latitudes around solar maximum. This is graphically displayed in the solar wind speed “dial plot” shown in Figure 1. In spite of large differences in solar wind statistics, if only the peaks in solar wind speed are considered these peak speeds show the same latitudinal dependence as the peak speeds at minimum, implying some rotation effect. The dynamic pressure at the recent solar maximum was only 50%-75% that at the last maximum, implying a smaller distance to the termination shock. Orbit II also expanded the determination of the different compositions and ionization states that occur in different types (slow, fast, transient) wind states.

Interplanetary magnetic field measurements in Orbit II go along with the plasma measurements at solar maximum in exhibiting alternating polarities to the highest latitudes, although the pattern is not random. A dipole-like character still dominates even at solar maximum and the dipole axis appeared to be approximately equatorial. Open flux was measured to be independent of latitude at maximum, as it was at minimum, and approximately equal to the open flux at the preceding sunspot minimum (Smith et al., 2003). This was discovered by extrapolating the radial magnetic field measured during the two fast latitude scans to a fixed radius and making the comparison.

Energetic particle events from the Sun, from interplanetary shocks, and from Jupiter that are seen near Earth are also seen at Ulysses, regardless of the position of Ulysses relative to the Earth. There is furthermore, to a greater or lesser degree, a disappearance of latitudinal, longitudinal, and radial gradients in particle fluxes near solar maximum. There is also virtually no latitudinal gradient in cosmic rays at solar maximum. This situation cannot be easily explained by existing models of energetic particle motion in the heliosphere. The drifts of charged particles is reversing in the second half of the solar magnetic cycle and it is hoped that measurements made then will produce a better understanding of what is leading to the easy latitudinal transport of particles.

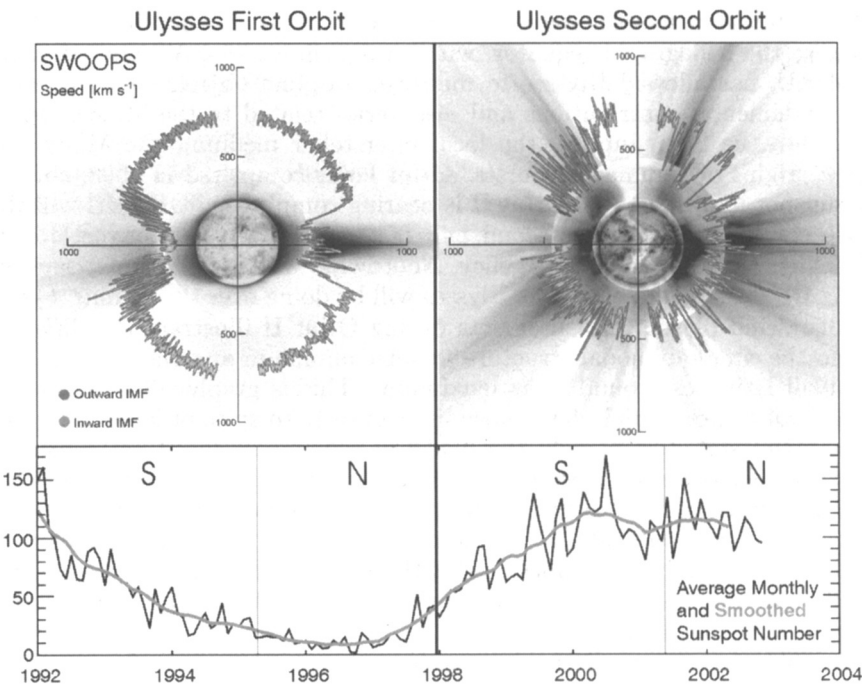


Figure 1. Polar plots of solar wind speed as a function of heliographic latitude for Ulysses' first two orbits. Sunspot number (bottom panel) shows that the first orbit occurred through the solar cycle declining phase and minimum while the second orbit spanned solar maximum. Both are plotted over solar images characteristic of (left) solar minimum (8/17/96) and (right) maximum (12/07/00); from the center outward images are from SOHO/EIT (Fe XII 195 Å), the Mauna Loa K-coronameter, and SOHO/LASCO/C2. (McComas et al., 2003)

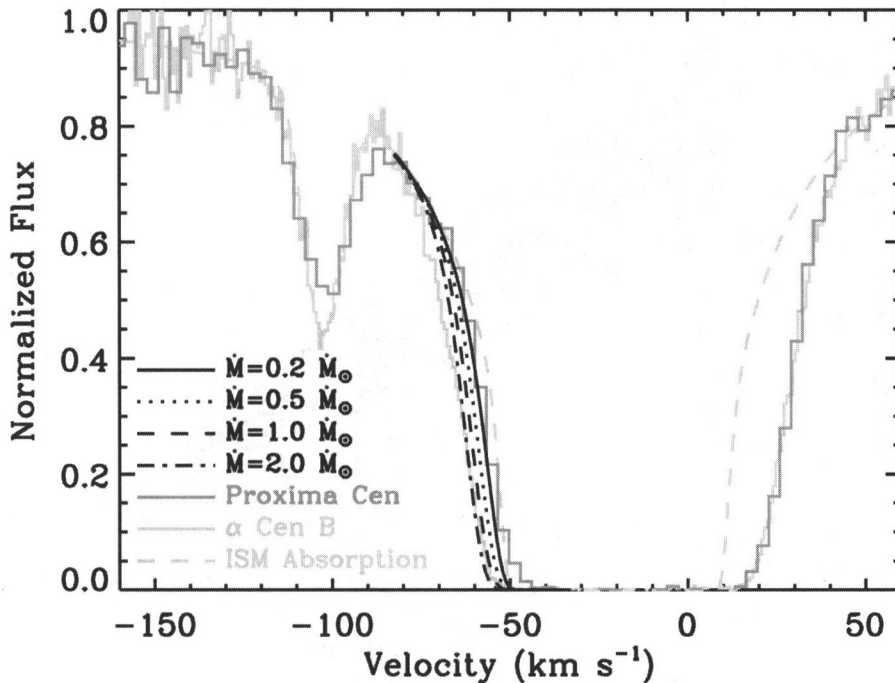


Figure 2. Empirical Lyman- α profiles for Proxima Cen and Alpha Cen B. The light-gray dashed line shows the interstellar absorption profiles of deuterium and metal lines. The extra absorption on the red side is heliospheric. The extra absorption on the blue side (different for the two stars) is astrospheric. Also shown are predictions of models for different mass loss rates. (from J. L. Linsky & B. E. Wood, *Space Telescope Sci. Inst. Newsletter*, December 2003)

3.2. Hydrogen Walls: Mass Loss of Dwarf Stars and the Young Sun

The collision of an ionized stellar wind with the partially-ionized warm gas in the interstellar medium creates a population of hot decelerated neutral hydrogen atoms. This “hydrogen wall” produces a blue-shifted absorption component in the stellar Lyman- α emission line that has now been detected in HST spectra of six dwarf stars. Figure 2 shows the Ly- α profiles for two of these stars. The blue side of the Ly- α absorption (-70 to -50 km/s) is different for these two nearby stars, leading to the estimates of the mass loss rates. The physics of this interaction, its understanding, based on similar processes occurring around the heliosphere, and progress in the observational program were reviewed by J. Linsky (Joint Inst. for Laboratory Astrophysics, Colorado, USA). Comparisons of the observed Lyman- α line profiles with theoretical models lead to the first very sensitive measurements of mass loss rates, as small as $4 \times 10^{-15} M_{\odot}/\text{year}$, for solar-like dwarf stars. The range of mass loss rates determined so far is $0.2 M_{\odot} \leq \dot{M} \leq 30 M_{\odot}$. The speed of the local interstellar plasma relative to the stellar wind source has been $25 \leq V_{ISM} \leq 130 \text{ km/s}$, where the heliosphere is moving at $\sim 25 \text{ km/s}$.

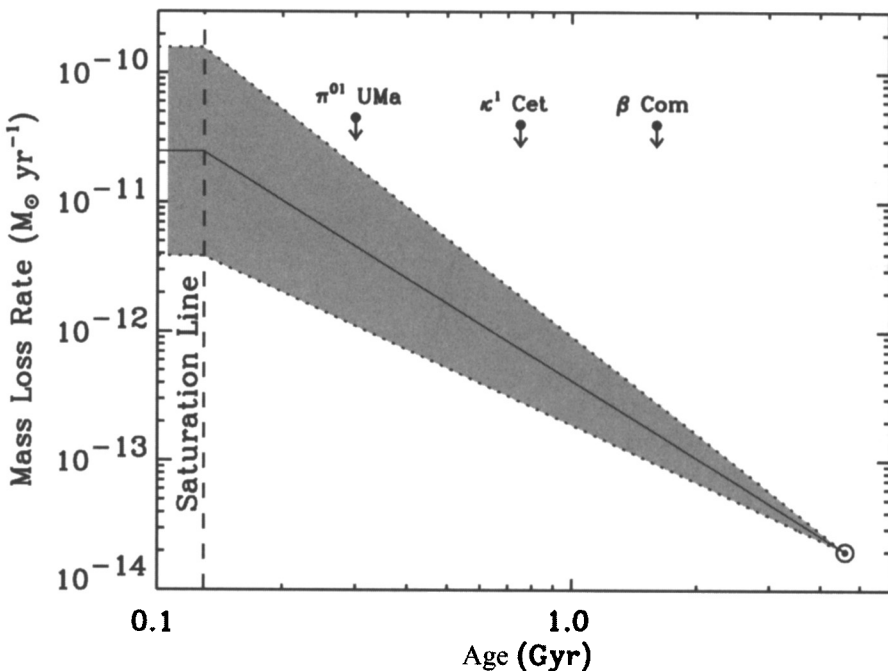


Figure 3. The mass loss history of the Sun, based on empirical mass loss rates for dwarf stars of different ages and X-ray surface fluxes. The upper limits are based on radio nondetections of three solar-like stars (Gaidos et al., 2000). (from J. L. Linsky & B. E. Wood, *Sky & Telescope*, in press, December 2003)

The observational program of Linsky and his colleagues provides the first observational data (other than for the Sun) with which to test theories for winds of solar-like dwarf stars. It shows an empirical correlation of stellar mass loss rate with X-ray surface flux that allows prediction of the mass loss rates of other stars and inference of the solar wind flux at earlier times, when the solar wind may have been as much as 1000-fold more massive. The solar prediction is shown in Figure 3. Important ramifications exist for the history of planetary atmospheres in the solar system - that of Mars in particular, and for exoplanets around stars.

In reference to the heliosphere, the volume of space dominated by the solar wind and its magnetic field, the regions dominated by these stellar winds and leading to their hydrogen walls, are called astrospheres. This naturally leads to a full set of corresponding terminology, including astropauses which divide stellar wind plasma from local interstellar plasma, bow and termination shocks, and inner and outer astrosheaths between the astropauses and the associated bow and termination shocks (Figure 2).

The models presently used to interpret the Lyman- α absorption normally assume the simplest possible wind: spherical symmetry and a speed of 400 km/s (Wood et al., 2000). As data accumulates on astrospheres, it will become possible to test these assumptions to examine, for example, whether the bimodal

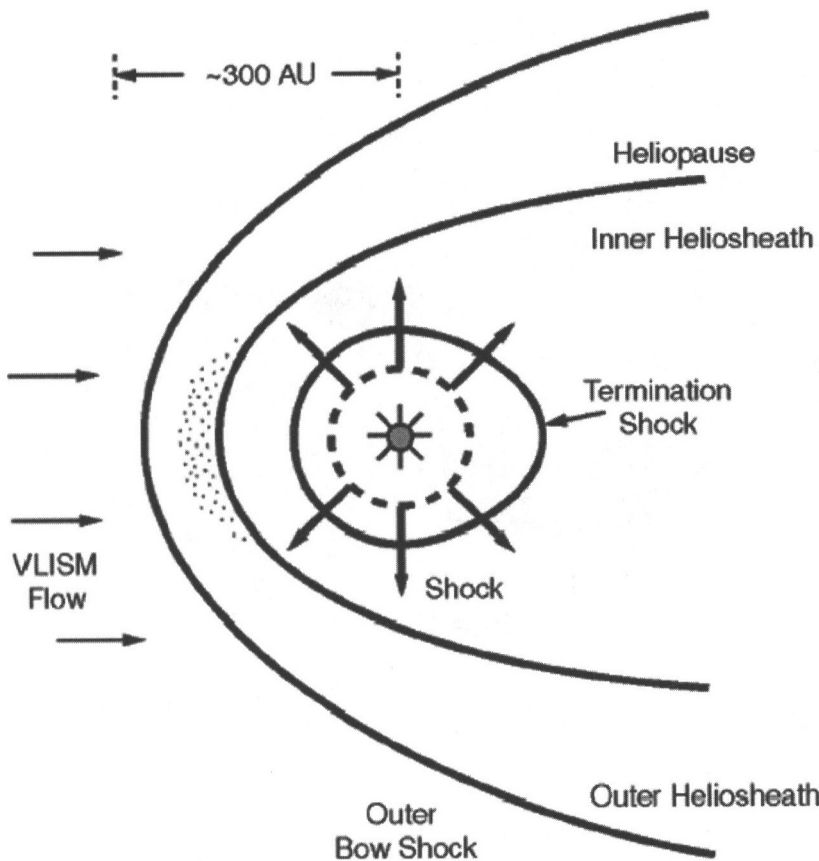


Figure 4. Plasma boundaries associated with the local interstellar medium - solar wind interaction. Stippling shows where lower-hybrid drive is predicted to occur, while the dashed line shows a GMIR shock moving toward the heliopause (Cairns and Zank, 2002).

nature seen in the solar wind around solar minimum (Figure 1) is more typical of dwarf star winds.

3.3. Radio Emission from the Outer Heliosphere and Beyond

The Voyager spacecraft have observed episodic bursts of radio emissions near 2-3 kHz that are generated beyond the inner heliosphere. These are believed to occur when shock waves driven by global merged interaction regions (GMIRs) reach the vicinity of the heliopause (see Gurnett et al., 1993). It is presently thought that the heliopause, which divides solar wind plasma from local interstellar plasma, lies roughly 150 AU from the Sun so that it takes a few years for GMIRs to pass through the heliosheath and reach the heliopause (Figure 4).

The Voyagers are traveling in a direction which is within a few tens of degrees of the upstream direction relative to motion of the heliosphere through

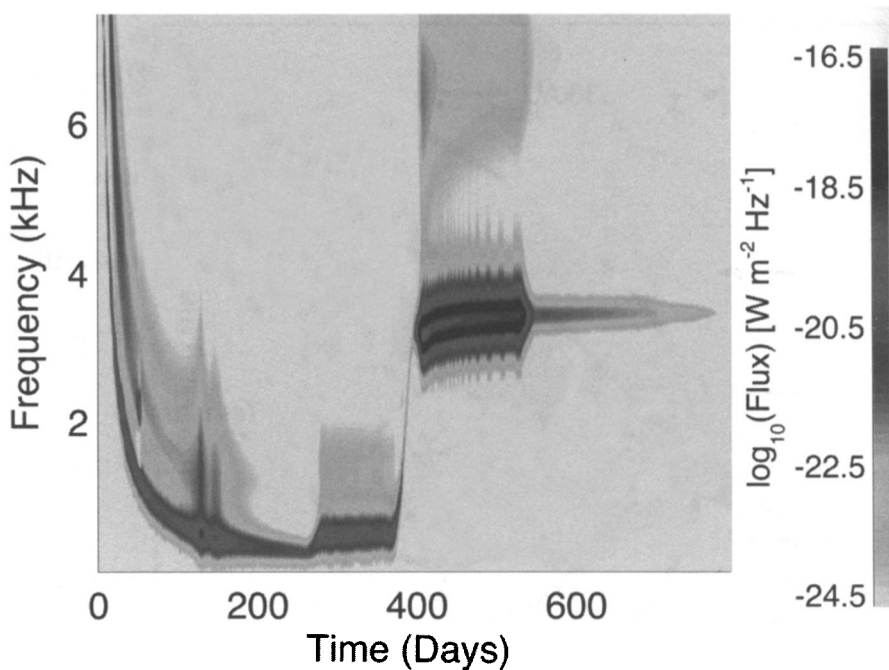


Figure 5. Theoretical prediction for the dynamic radio spectrum (J. Mitchell, I. Cairns, & P. A. Robinson, JD 07 Poster Paper).

the local interstellar medium and are expected to soon encounter the termination shock. They are the only spacecraft that are far enough from the Sun to be able to detect such low-frequency emission originating in the outer heliosphere or beyond. Amplitude and time-of-flight measurements and use of occasional spacecraft roll testing to study modulation of the signal, indicate the source is in the vicinity of the nose of the heliosphere. More concisely, the source seems to start at the nose and migrate away along a line lying near the galactic plane.

Voyager observations and theories for the source region, generation processes, and propagation of the radiation were reviewed in this presentation by I. Cairns (Univ. of Sydney, Australia). Special foci were the successes of the current GMIR model for the radiation and a new theory which specifically addresses the turn-on and generation of the radiation in the outer heliosheath, near the heliopause nose, and the propagation of the radiation into the inner heliosphere.

The theoretical model (Cairns & Zank, 2002) predicts that the radiation is generated in the fore-shock region. It turns on when a GMIR shock enters a region primed with a supra-thermal electron tail beyond and near the heliopause nose. The tail is produced by “lower hybrid-drive” associated with pick-up ions. The model source mechanism explains how the supra-thermal electron tail increases the emitted radio flux and predicts that emission is predominantly at the fundamental plasma frequency (Figure 5). There is also a suggestion that the local galactic magnetic field lies mainly near the galactic plane (Figure 6).

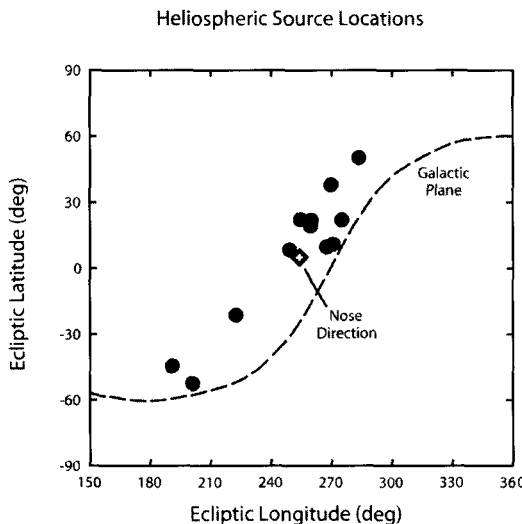


Figure 6. The direction to the low frequency radio source locations and the nose of the heliopause, suggesting the direction of the magnetic field in the local interstellar medium (Kurth et al., 2003).

The hypothesized source mechanism depends on interstellar neutral atoms being ionized in the vicinity of the heliospheric bow shock and then charge-exchanging with shocked solar wind plasma. One of the posters (Mitchell et al.) for this JD provided details on this source mechanism.

3.4. MHD Turbulence in the Heliosphere

The heliospheric plasma is an excellent laboratory to study the behavior of collisionless MHD turbulence. This is a topic of fundamental importance for both plasma physics and astrophysics and has been reviewed here by B. Bavassano (CNR, Italy). In the 1970s and 1980s decades impressive advances were made in the knowledge of turbulent phenomena in solar wind, although spacecraft observations were confined within a small latitude belt near the solar equator. In the 1990s, with the Ulysses mission, investigations have been extended to the high-latitude heliosphere. This has allowed studies of how the MHD turbulence evolves in polar solar wind, a plasma flow in which the effects of large-scale inhomogeneities are considerably less important than in low-latitude wind, at least near solar minimum when stable high speed wind dominates the polar heliosphere. With this new laboratory, important new results have been obtained. In the review, observations of turbulence evolution in polar wind were discussed and compared to those typical of the low-latitude solar wind.

Equatorial solar wind turbulence appears to normally have a strongly Alfvénic character, as determined by the coherence between solar wind plasma flow vector and magnetic field vector fluctuations. The power density spectrum of the fluctuations displays a characteristic $-5/3$ power law above a well-determined frequency which, in turn, moves downwards to lower frequencies with increasing distance from the Sun. Alfvénic modes are commonly described in terms of “Elsässer variables” (Marsch, 1991) \mathbf{z}_\pm describing outward (+) and inward (-) waves.

It was realized very early that the solar wind is expanding at speeds in excess of the local Alfvén speed beyond $\sim 5 - 30R_\odot$. The radius at which the Alfvén speed is exceeded is known as the Alfvén radius, r_A . Outside r_A both the \mathbf{z}_+ and the \mathbf{z}_- modes originating inside r_A are carried away from the Sun. Any inward mode beyond r_A must be of local origin, and therefore a consequence of nonlinear interactions or interaction of outward modes with the ambient gradients in the wind. Outward modes have been found to dominate in all regions. However, the difference decreases with increasing distance to show there are local sources of inward modes. These results all were gathered near the heliographic equator in a region of mixed solar wind states.

Figure 1 shows that the polar wind around solar sunspot minimum is fast and steady, as compared to wind near the heliographic equator. This presented the opportunity to study how Alfvénic turbulence evolves under undisturbed conditions. Power spectra in the solar minimum polar wind indicate a $-5/3$ spectrum similar to that measured in the equatorial wind, and that the spectrum also evolves towards lower frequency with increasing distance. A specific difference is that this spectral evolution with distance is slower than in low-latitude wind. A related result is that the predominance of outward modes continues to greater distances at high latitudes.

It is concluded that solar wind turbulence, in addition to having solar sources, is locally generated at velocity shear layers. Empirical results also show that the presence of magnetic field reversals speeds up spectral evolution. This process may have a relevant role in increasing the rate of turbulence evolution in low-latitude solar wind where fast-slow stream structures and reversals of the magnetic polarity are common. In the polar wind, where velocity gradients are weak, other mechanisms have to exist and parametric decay has been proposed. This is presently one of the main areas of investigation.

4. From the Transition Region to the Corona and Beyond

4.1. The Magnetic field from the Sun to the Interstellar Medium

The behavior of the magnetic field from the interior of the Sun out to the interplanetary medium has been reviewed by S. Solanki (Max Planck Institute for Aeronomy, Germany) who began by describing the recent observational evidence about large scale flow fields and the internal rotation velocity of the Sun, which supports an overshoot-layer dynamo scenario. Magnetic flux tubes in the overshoot region reach the surface of the Sun when subject to undular instability and emerge with properties (tilt angle, latitude of emergence) that are observed in active regions (Caligari et al. 1995). Numerical MHD simulations of the magnetic field dynamics in plage regions are being developed and reproduce

reasonably well the observed morphological patterns and measured quantities (Vögler & Schüssler 2003).

Solanki proceeded then to discuss how the magnetic field acts as the coupling agent between higher and lower solar layers, the latter being responsible for the structure and energetics of the overlying levels. A beautiful example of this is offered by 3-D numerical simulations that show how displacements of the photospheric footpoints of magnetic loops result in a magnetic dissipation strong enough to heat and maintain loops at coronal temperatures (Gudiksen & Nordlund 2002). Observational evidence of electric current sheets at coronal base have been obtained via He I 10830 Å line data.

At high coronal altitudes the magnetic field can be modeled by extrapolating photospheric values under different assumptions: the reconstructed coronal field is then compared with LASCO white light images. Far away from the Sun, the interplanetary field configuration had been predicted by Parker. More recently, Fisk extended Parker's model taking into account the misalignment between the magnetic and the rotation axis as well as the loop footpoint motions. The model better reproduces the cosmic rays behavior (Fisk 1996).

A relevant question to ask is whether the changing magnetic fields at the solar surface are the source of the variability of the solar irradiance and whether this variability accounts for the earth climate changes. Solar variability can be reconstructed by properly modeling the quiet sun, the sunspots and faculae evolution over time. However, climate changes, as recorded by the temperature increase measured after 1970, cannot be ascribed to changes in the solar irradiance, which is at most responsible for a fraction of the order of $\approx 30\%$ of the observed behavior (Krivova et al. 2003, Solanki & Krivova 2003).

4.2. The 3D Solar Wind Over the Solar Cycle Observed by IPS

M. Kojima (STE Lab., Nagoya Univ., Japan), reported on the 3-D solar wind properties over the solar cycle, as derived from interplanetary scintillation measurements (IPS), in a review co-authored by M. Tokumaru, K. Fujiki and M. Hirano (STE Lab., Nagoya Univ., Japan), B. V. Jackson and P. Hick (CASS, Univ. of San Diego, USA), K. Hayashi (W.W. Hansen Experimental Physics Lab., Stanford Univ., USA) and T. Ohmi (Science and Technology Dept., CTI Co., Ltd.). Because interplanetary scintillation observations integrate along the line-of-sight, data need to be analyzed with a tomographic technique in order to retrieve the three dimensional wind parameters (see, e.g. Hayashi et al. 2003). Kojima showed that the solar wind speeds derived from a recently developed IPS tomographic technique compare well with *in situ* values measured by Ulysses. Figure 7 illustrates IPS results over 14 Carrington rotations and gives corresponding Ulysses values.

With this method, Kojima and collaborators have been able to study the solar cycle dependence of the solar wind properties, such as the speed of the wind, the asymmetry of fast wind, the origin of the slow wind, the bimodal character of the wind. IPS studies show also that the Nolte et al. (1976) claim (later supported by Neugebauer et al. 1998) that the smaller a coronal hole, the lower the solar wind speed originating from the hole, is only a first approximation to a more complex behavior. For instance, slow wind may emanate from a small coronal hole close to an active region, at solar minimum, as well as it

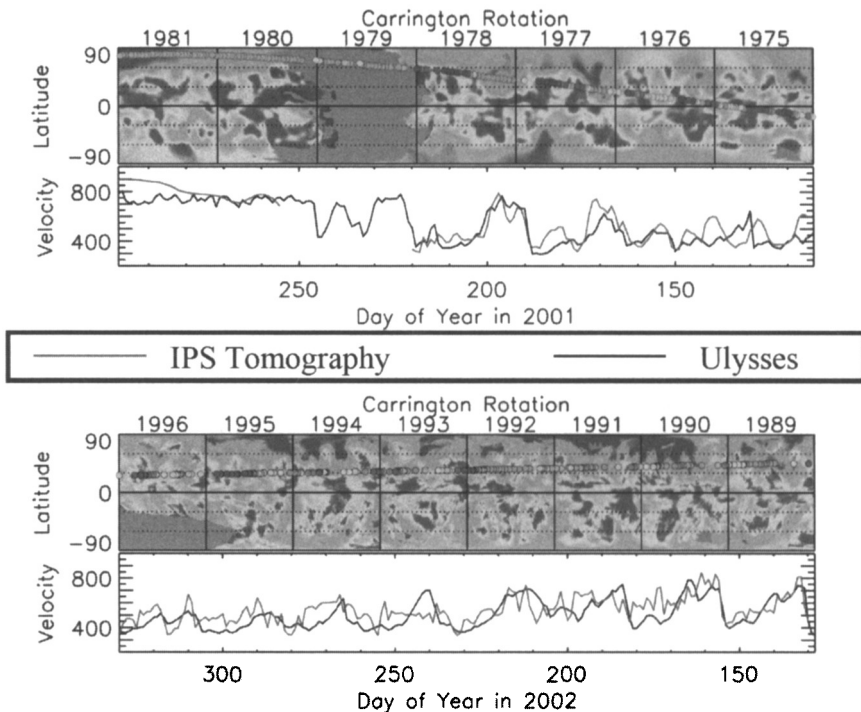


Figure 7. Solar wind speed measured over 7 Carrington rotation in years 2001 and 2002 as derived from IPS tomography are compared with speeds measured *in situ* by Ulysses.

emanates from a small polar hole, at solar maximum (Ohmi et al. 2001, Ohmi et al. 2003). Also, during the ascending phase of the solar cycle, wind streams originating from holes that shrink from a large to a smaller area do not change their speed. Obviously, the same behavior occurs in descending phases of the solar cycle.

Impressive solar wind "images", giving the distribution of the solar wind speed all over the solar surface, throughout the solar cycle, may be built from IPS data. The solar cycle in solar wind may be compared with conventional images of the solar cycle in magnetic fields or in solar X-rays, as directly observed by, for instance, NAO and Yohkoh instrumentation, respectively. These maps provide an immediate first-order answer to questions such as the sources of slow/fast wind, the percentage of solar surface they occupy, and their dependence on the solar activity distribution.

On the basis of the measured wind speed, it has been possible to reconstruct the profile of the solar wind speed *vs.* latitude. Depending on the phase of the solar cycle, the fast wind latitudinal velocity gradient $dV/d\theta$ varies between zero and $4 \text{ km s}^{-1} \text{ deg}^{-1}$. The bimodal character of the wind, already identified in Ulysses observations, is reproduced quite well by IPS measurements. The

bimodality holds in the ascending and descending phase of the solar activity cycle and not only at minimum activity (Kojima et al. 2001).

It is well known that the wind speed seems to correlate well with the expansion factor of its source region f (see, e.g. Wang and Sheeley 1990) and/or to its photospheric magnetic field B (see, e.g., Fisk 1996). On the basis of the wind speeds measured by IPS, of the average magnetic field measured at photospheric levels over the wind originating region and of the flux expansion rate calculated from potential extrapolations, Kojima showed that neither the Wang and Sheeley, nor the Fisk assumption, are valid. The correlation factor between the wind speed and the magnetic field is on the order of 0.4 — 0.5, while the correlation factor between the speed and the $1/\sqrt{f}$ factor suggested by Wang and Sheeley is ≈ 0.7 . However, the correlation factor rises to 0.91 ± 0.1 , when the wind speed is compared to B/f values.

Also time—dependent phenomena, like coronal mass ejections (CMEs), can be studied via IPS measurements, adopting the time-dependent tomography algorithm developed to this purpose (see e.g. Jackson et al. 2003). This new program will be applied also to the study of the evolution of co-rotating heliospheric structures. Preliminary results are very promising and will be used for reconstructing in three dimensions the evolution and interaction of interplanetary structures.

4.3. The Energy Balance from the Chromosphere to the Corona and its Effect on Solar Wind Properties

While Solanki's talk focused on the role of magnetic fields from the Sun to the interplanetary space, O. Lie-Svendsen (Norwegian Defence Research Establishment) showed how the flow of energy between the chromosphere and the corona controls solar wind properties. That the solar atmosphere is the source of the solar wind and the heliospheric plasma is obvious, but the coupling occurs via processes which are not yet well known. In particular, one should understand how energy is fed into the coronal and solar wind plasma and how the upper chromosphere reacts to the downward energy flow from the hot corona.

Lie-Svendsen illustrated results from a solar wind model which has its lower boundary in the chromosphere and its upper boundary at 1 AU. The model, based on the 16—moment transport equations developed by Demars & Schunk (1979), uses the gyrotropic approximation to these equations deriving densities, the drift speed along the magnetic field, the temperatures and the heat flux densities parallel and perpendicular to the magnetic field, for each particle species. Details of the model characteristics (e.g., terms adopted in the description of coronal and chromospheric heating) can be found in Lie-Svendsen, Hansteen, & Leer (2002), Lie-Svendsen, Hansteen, Leer & Holzer (2002).

The study addresses the questions of how the energy transport between the lower atmospheric levels and the corona, as well as the energy deposition in the transition region, affect the solar wind characteristics out to 1 AU. Both a radial and a super-radial geometry are considered and the properties of the resulting two solar wind "modes", namely fast and slow solar wind, are illustrated in Figure 8. It should be pointed out that the use of higher order transport equations, and the description of the collisionless plasma, has been crucial in establishing the characteristics given in the figure, and also revealed how the altitude inter-

Two solar wind “modes”

	slow	fast
geometry	radial	rapidly expanding
<i>downward heat flux absorbed by</i>	<i>radiation</i>	<i>enthalpy flux</i>
wind speed	slow	high
solar wind mass flux	high	low
coronal density	high	low
heat flux	classical	non-classical
transition region pressure	high	low
mass flux limited by	coronal heating	transition region heating (supply from chromosphere/transition region)
coronal He abundance	high	low
He mass flux limited by	coronal energy	supply from chromosphere (a problem!)

Figure 8. Main properties of slow and fast wind as derived in the model presented by Lie-Svendsen (see text).

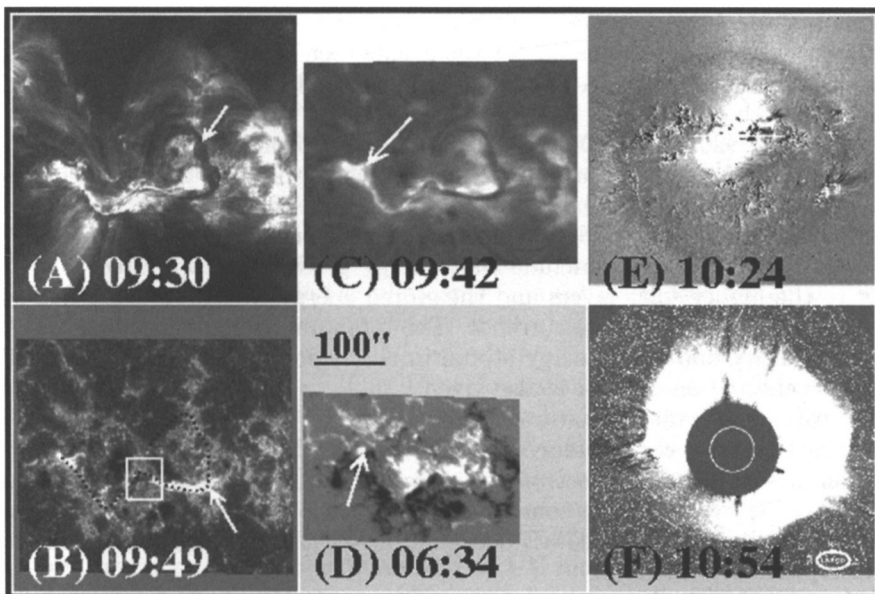


Figure 9. The Bastille day event scenario: (A), (B) *TRACE* images in, respectively, 195 and 1600 Å (C) H_{α} filtergram about 20 minutes before the X5.7 flare occurrence, (D) line of sight magnetogram of the Bastille event region, from Huairou Solar Observing Station, (E) running difference of SOHO EIT images at the time of flare maximum, (F) running difference of LASCO C2 images at the time it first detection in C2 (Zhang et al., 2001).

val (somewhere in the transition region or low corona), where plasma changes from being collisional to being collisionless, although fairly limited, has a large influence on the solar wind mass flux: a good example of the solar-heliospheric connection! However, additional work may be necessary to insure that the model realistically describes the proton velocity distribution in the extended corona, as the model assumes a not too large departure from a bi-Maxwellian function.

4.4. The Bastille Day Event: From Solar Surface to the Far Heliosphere

An example of a solar event whose effects have been detected and measured out to ≈ 60 AU has been presented by J. Zhang (National Astronomical Observatory, Chinese Academy of Sciences), who summarized the observations of the so called *Bastille Day Event*, from the solar surface to the outer interplanetary space. This event occurred on July 14, 2000, and his manifestations include a giant filament eruption, a large flare (X5.7/3B) and an earth-directed coronal mass ejection. Figure 9 shows pre and post flare images of the Bastille event region as imaged by different experiments (Zhang et al. 2001).

Observations of the magnetic evolution of the active region (NOAA 9077) where the flare occurred revealed multiple cancellation events (or slow reconnection events) in the vicinity of the filament bridging the region. These obser-

vations provide evidence of the role played by slow reconnection in generating the global instability responsible for the events seen in the region. Over a more extended area, a large transequatorial filament, and loop arcade, appear to be associated with the CME.

Yan et al. (2001) and Deng et al. (2001) have been able to reconstruct the magnetic configuration of the region above the photosphere via a non linear force free field extrapolation of the vector magnetic fields measured at the Huairou Solar Observing Station (HSOS). From the evolution of the non-potentiality of the region these authors conclude that energy gradually propagated from the lower to the higher solar layers and the stored energy caused first the filament eruption and then the flare occurrence. The temporal profile of the longitudinal current, helicity and total energy stored in the region over a time interval of a few days centered on July 14 is also given.

A variety of radio signatures were associated to the 14 July event. In particular the flare event produced an intense, long duration Type III-like radio emission, associated with electrons accelerated deeply in the corona (Reiner et al. 2001). The CME was the source of Type II radio emission, whose frequency drift indicated a significant CME deceleration, as it moved from the corona to the interplanetary medium.

Near 1 AU the solar wind structure associated with the Bastille event consisted of a large speed stream observed on July 15 and a few small streams. Over a period of 6 days the wind speed increased from 400 to 1100 km s^{-1} and the field from 10 nT to 60 nT . An interaction region, bounded between a pair of forward and reverse shock has also been identified (Whang et al. 2001). The CME-driven shock arrived at *Voyager 2*, at $\approx 63 \text{ AU}$ on January 12, 2001, with a speed jump of 60 km s^{-1} . These observations provided a good opportunity to study the shock propagation from the inner to the outer heliosphere: MHD simulations showed that the CME shock changed dramatically in strength and propagation speed as it moved outward (Wang et al. 2001). The leading forward shock has decayed while all other shocks and discontinuities apparently dissipated by the time they would have reached *Voyager 2*. The merged interaction region had expanded to at least 10 days in length.

The response of the Earth's inner magnetosphere to the Bastille CME has been recorded by the IMAGE spacecraft, which made images in the Energetic Neutral Atoms (ENA) produced by charge exchange between the hot magnetospheric ions and the cold geocoronal neutral hydrogen. These images showed that as the B_z component of the interplanetary magnetic field became positive the ring currents became closed and symmetric (Brandt et al. 2001). A large polar cap absorption event, lasting about 3 days, has also been observed at the Zhongshan station, in Antarctica (Liu et al., 2001) and large geopotentials had been induced over oceanic distances (Lanzerotti et al. 2001).

Optically, the Bastille day event was the fourth event in solar cycle 23 that had an optical importance of 3B. Although larger events had been observed in other solar cycles, it was undoubtedly an extremely large event and it provided a good opportunity to study the different manifestation of large events throughout the solar atmosphere and the heliosphere. We point out also that the study of the return period of such events is relevant for the prediction of natural hazards in space weather.

5. Energetic Particles, Energetic Neutral Atoms, and Composition

5.1. Elemental Abundances in the solar Corona

J. Raymond (Harvard-Smithsonian Center for Astrophysics, Cambridge, USA) reviewed our present knowledge of elemental Abundances in the solar corona and pointed out how many analyzes of astrophysical observations assume "solar elemental abundances" without recognizing the large variations of abundances within the solar atmosphere. However, abundances in the solar corona are modified with respect to those in the photosphere in (at least) two systematic ways. First, the abundances of elements whose neutral species have an ionization potential below about 10 eV are enhanced relative to elements whose atoms have higher ionization potentials. This First Ionization Potential (FIP) effect has been studied for many years, and it is typically a factor of 3 or 4 enhancement. The second effect is a reduction of the abundances of all elements relative to hydrogen. It has been less well studied because hydrogen lines or continuum are not found in the wavelength ranges of many instruments, or else the lines are optically thick or formed at different temperatures. Recent studies of line/continuum ratios in solar flares and of UV line intensities above the solar limb have begun to remedy this problem, and depletions of order a factor of 3-10 are commonly observed. They are attributed to gravitational settling.

Abundances also have important physical consequences. The radiative cooling rate is directly proportional to the abundances at temperatures up to about 10^7 K, where bremsstrahlung begins to dominate. The mean particle weight can affect flow dynamics, and Hansteen et al (1997) have studied the effects of helium on the fast solar wind. Moreover, preferential acceleration of oxygen is observed in the fast solar wind and attributed to cyclotron damping of plasma waves (Cranmer et al. 1999). While the oxygen abundance is too small to have much of an effect on the overall dynamics of the wind, analogous preferential heating of helium could have major consequences.

Most coronal abundance determinations rely upon ratios of collisionally excited emission lines. One can obtain the relative abundances of two elements by choosing spectral lines such that the product of excitation rate and ionic concentration has the same temperature dependence for both lines. A common example is the Ne VI and Mg VI lines near 400 Å which has the additional advantage that the wavelengths are so close that the instrumental radiometric calibration uncertainty also cancels out. In the X-ray range, O VIII Ly α and the nearby lines of Fe XVII are formed at similar temperatures. There is never a perfect match of temperature response, and time-dependent ionization could distort the derived abundances, but in general these methods give reliable relative abundances within the uncertainties in the atomic rates.

To carry the analysis a step further, one can obtain absolute abundances if one of the elements being compared is hydrogen. This can be difficult, in that there are no lines of hydrogen shortward of 912 Å. The bremsstrahlung continuum is largely formed by hydrogen, and it can be measured shortward of about 10 Å. Absolute abundances in solar flares can be derived by measuring the equivalent widths of lines such as Ca XIX $\lambda 3.18$, provided that that ion dominates at the temperature of the flare plasma and that the continuum is not contaminated by fluorescence due to X-rays at shorter wavelengths (Fludra &

Schmelz 1999; Phillips et al. 2003). For observations of the corona above the limb, the hydrogen Lyman lines can be compared with lines of other elements. The analysis is somewhat different in the Lyman lines that include strong contributions from radiative scattering, but results have been obtained for coronal holes, active regions and streamers (Raymond et al. 1997; Feldman et al. 1998; Laming & Feldman 2003; Ko et al. 2002; Bemporad et al. 2003)

Overall the observations show a FIP enhancement that varies not only from one region to another, but also increases with time within individual active regions as they evolve (Widing & Feldman 2001). The gravitational settling effect seems to be observed in the closed field regions of active region streamers and equatorial streamers at solar minimum.

Various explanations have been proposed for the FIP effect, but all agree that it must occur in the chromosphere (see review by Henoux 1998). Models include diffusion (Peter 1998), rising magnetic fields and injection of enriched material by reconnection (Arge & Mullan 1998). Gravitational settling has a characteristic time scale of about 1 day. In a steady state, gravitational settling would predict much smaller abundances than observed (Lenz, Lou & Rosner 1998), suggesting continual mixing of fresh material.

5.2. The Heliospheric Interface: Theory and Observations

Sun is moving through warm (\sim 6500 K) and partly ionized local interstellar cloud (LIC) with velocity \sim 26 km/s. The charged component of interstellar medium interacts with the solar wind (SW) forming the heliospheric interface, the SW/LIC interaction region (Figures 4, 10). Both the solar wind and interstellar gas have a multi-component nature that creates a complex behavior of the interaction region. The current state of art in the modeling of the heliospheric interface was reviewed by V. Izmodenov (Moscow State University, Russia). Modern models of the interface take into account effects of the solar wind and interstellar plasma components (protons, electrons, pickup ions, interstellar helium ions and solar wind alpha particles), interstellar neutral component (H atoms), interstellar and heliospheric magnetic fields, galactic and anomalous cosmic rays, latitudinal and solar cycle variations of the solar wind. New results of self-consistent time-dependent kinetic/gas-dynamic model of the heliospheric interface were reported. Predictions of the theoretical models were compared with available remote diagnostics of the heliospheric interface - backscattered solar Lyman- α radiation, pickup ions, deceleration of the solar wind at large heliocentric distances, heliospheric absorption of stellar light, anomalous cosmic rays (ACRs) and heliospheric neutral atoms (ENAs).

Remote diagnostics of the interface region include observations of pickup ions created from interstellar atoms, solar Lyman- α radiation that is backscattered from interstellar neutral atoms, and the kilohertz radio emission discussed above in §3.3, where models of the radio emission were described. Global interactions are the focus here. The models are typically either multifluid or kinetic hybrid, but not both, and are often not well determined in that they still make somewhat different predictions. They are, however, uniform in predicting that the effect of interstellar neutrals is large, reducing the radius of the termination shock from 200 to \sim 100 AU. These neutrals are also the source of the hydrogen wall (§3.2, Figure 10(b)). The models show that the heliotail extends far

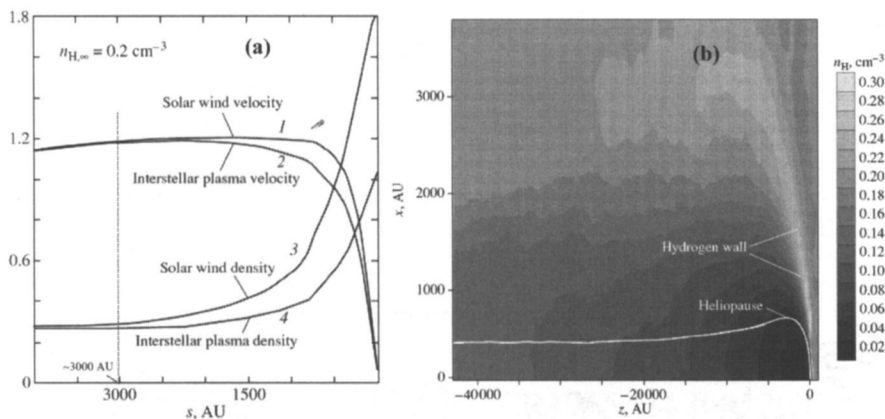


Figure 10. (a) Density and flow speed in the interstellar medium and far down the heliotail, showing when the two finally merge. The velocities and densities are normalized to their interstellar values (Izmodenov & Alexashov, 2003). (b) The two-dimensional density distribution of hydrogen atoms in the heliospheric interface. At heliocentric distances $\sim 40,000$ AU, the atomic density is close to its value in the unperturbed interstellar medium. The hydrogen wall, the increase in the density of hydrogen atoms in front of the heliopause, is clearly seen. The intensity of the hydrogen wall decreases with increasing heliocentric distance.

out to $\sim 2000 - 3000$ AU where the heliopause finally disappears due to charge exchange effects. The heliotail does not disappear, but extends indefinitely in models without neutral interstellar hydrogen (Figure 10(a)).

Other model predictions are that the heliosphere, overall, breathes in and out with the solar cycle, as the solar wind dynamic pressure changes (§3.1, Figure 11). The distance to the termination shock varies by $\sim 20\%$ and shock waves between the heliopause and bow shock can sometimes be induced in the simulations.

The models are now being used to investigate modulation of galactic cosmic rays (GCRs) in the inner and outer heliosheaths and their general access to the heliosphere. GCRs are found to have only a minor effect on the termination shock. Conversely, the models indicate that GCRs have an important effect on the boundary region and, in turn, are strongly modulated in the boundary region.

5.3. Propagation of Energetic Particles to High Latitudes

Trevor Sanderson (European Space Agency, Noordwijk, The Netherlands) illustrated how the Ulysses mission has taught us that the heliosphere can no longer be considered as a uniform entity - that any study of the propagation and acceleration of particles in the heliosphere must take into account the three-dimensional structure. The starting point for this discussion was again the bimodal structure of the solar wind around solar sunspot minimum, illustrated in Figure 1. The propagation of energetic particles at low latitudes in low speed solar wind is

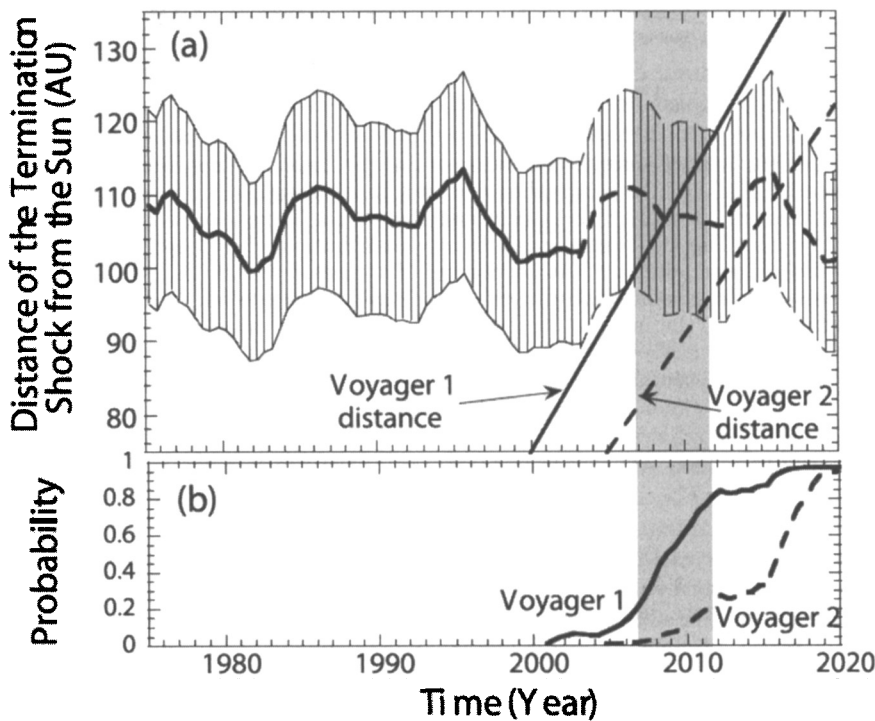


Figure 11. (a) Mean, with $1-\sigma$, of the termination shock distance (in astonomic units) as a function of time, at 30° from the upwind direction (Izmodnov et al., 2003). (b) Probability of termination shock crossing for Voyager 1 and Voyager 2 as a function of time.

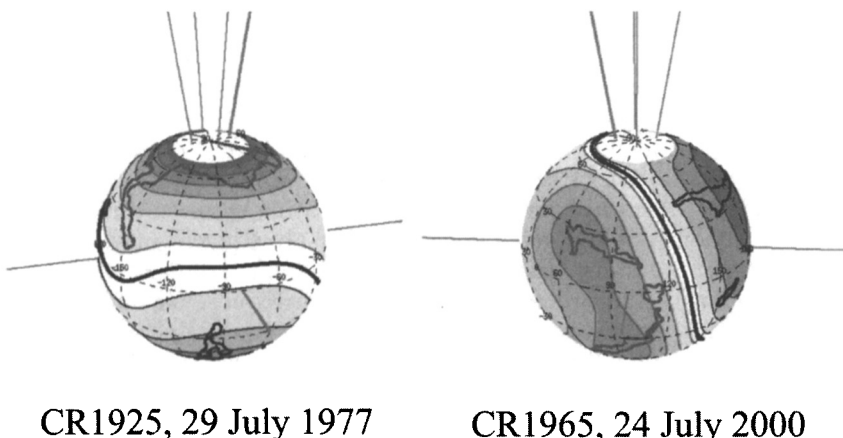


Figure 12. Source surface maps of the coronal magnetic field strength and direction.

influenced by the presence of small scale structures such as discontinuities and large scale structures such as CIR's, CME's, and transient stream interaction regions. High latitude wind near solar minimum differs considerably. It is high speed, contains large amplitude Alfvén waves and a relative deficit of CIR's and CME's. Low latitude energetic particle events interacting and originating from these structures were then described (e.g., Lanzerotti & Sanderson, 2001). Based on ISEE-3 35-1600 keV ion observations, typical behavior is for: (i) Upstream ion flux to increase as a shock approaches. (ii) Upstream ions to resonate with upstream waves. (iii) Ion flux to peak \sim 6 hours after the shock. (iv) Ion flux to drop within CMEs. (v) Ion distributions to be bi-directional within a CME.

Around solar sunspot maximum, solar wind conditions are considerably different (Figure 1). The streamer belt is highly inclined, coronal holes are small, and there is little high speed wind near the ecliptic plane (Figure 12). During the second high latitude pass of Ulysses, near solar maximum, several energetic particle events at high latitude and in high speed solar wind flow were observed, with energies extending from \sim 1 to \sim 100 MeV. The high speed wind arose from small coronal holes that were beginning to form just after solar maximum. These particle events, observed for the first time under such conditions, give us the opportunity to study particle propagation within the substantially different conditions of the fast and slow solar wind. Sanderson presented a detailed analysis of particle time-intensity profiles and anisotropies in the relatively homogeneous plasma of the high speed flow. He compared these events with events observed in the slow solar wind, and discussed this in the context of current propagation models. These high latitude events, all associated with CMEs in the high speed wind, presented a different character than corresponding low latitude events: (i) The ion flux peaks at the leading edge of the CME, not at the shock. (ii) The ion flux is higher within the CME. (iii) There are no bi-directional ions within the CMEs. These high latitude CMEs are usually 'over-expanding' and will be a target of study during the third Ulysses orbit.

5.4. Particles in the Heliosphere: An Overview

While J. Raymond's talk focused on elemental abundances in the solar corona, and gave estimates of the present solar abundances, R. Wimmer-Schweingruber (Institut für experimentelle und angewandte Physik, Kiel, Germany) dealt with an historical perspective of solar and heliospheric abundances. This is a fascinating subject, which has the capability of creating cross-cultural exchanges between "astronomers" and geophysicists. Solar abundances may vary during the Sun lifetime: we know that the Sun formed from an interstellar medium, $\approx 4.5 \cdot 10^9$ years ago, and processes, like supernovae explosions, and events, like embodying planets at an early stages of its life, have an impact on solar abundances. Knowledge of solar abundances thus may provide us with information about the composition of the primitive nebula - an essential issue for the understanding of planetary system formation and evolution.

Helioseismology data provide a means to get information about inhomogeneities in the composition of the interior of the Sun via a comparison between measured and predicted oscillation modes (we remind the reader that the speed of sound depends, among various factors, on the mean molecular weight of the plasma). These analysis suggested that the photospheric abundance of elements heavier than H decreased by $\approx 10\%$ over the sun lifetime, because of the gravitational settling of heavier elements. This reduction is too small to be tested by photospheric abundance measurements and Wimmer-Schweingruber described an alternative way to check the predicted variation by a comparison between abundances in meteorites and in the solar wind (Turcotte & Wimmer-Schweingruber 2002).

Chondritic meteorites are assumed to keep a record of the composition of the pre-solar nebula. Abundances in meteorites thus give a fairly accurate description of solar abundances and can be measured with a higher accuracy (3 - 10 %) than photospheric abundances (which are known with an uncertainty of at least 25 - 30 %, this being the uncertainty of atomic parameters alone). A comparison between meteoritic and photospheric abundances is given in Figure 13. Wimmer-Schweingruber then showed that abundances in fast wind, because of their small First Ionization Potential (FIP) effect, are best suited for a comparison with meteoritic abundances and that the isotopic composition of fast wind is best representative of the plasma feeding the wind.

Another means to test the predicted behavior of solar abundances with time calls for an analysis of lunar soil. Heber et al. (2003) have analyzed lunar samples of different solar wind antiquities, that is samples exposed to solar wind in different epochs. Results from the Heber et al. work seem to indicate a time evolution of the ${}^3He/{}^4He$ ratio in solar wind, which might be interpreted as an effect of gravitational settling of the heavier 4He or of some mixing of 3He produced by incomplete H burning beneath the convection zone. However, a more thorough analysis revealed the increase of the ${}^3He/{}^4He$ ratio to be an artifact and the authors conclude that lunar samples point to a constant ${}^3He/{}^4He$ ratio in solar wind over the past ≈ 4 Gyr.

At a greater depth than used for measuring solar wind particles, lunar soil shows the presence of particles more energetic than found in solar wind, which, in spite of being dubbed *SEP* (Solar Energetic Particles) are much more abundant than today's solar energetic particles and cannot be ascribed to en-

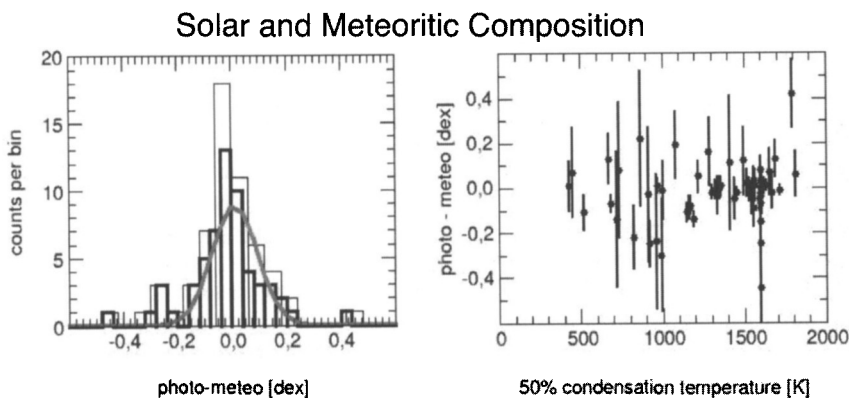


Figure 13. Comparison between meteoritic and photospheric abundances normalized to Mg. Right panel: the logarithm of the abundance ratio X/Mg in meteorites divided by its corresponding photospheric value is plotted vs. $1/2$ the condensation temperature. Left panel: the same as the left panel plotted as a histogram and fitted by a Gaussian with a standard deviation of 0.084 dex.

hanced solar activity in the past. This *SEP* component, according to Wimmer-Schweingruber, has a non-solar origin and can be ascribed to interstellar pick-up ions (PUI) ionized and accelerated in the heliosphere. This interpretation of the *SEP* population opens up the possibility of using the lunar soil as an historical record of the galactic environment the Sun has encountered during its lifetime (Wimmer-Schweingruber & Bochsler 2001, 2003). New instruments that measure the composition of the solar wind and of supra-thermal and energetic particle populations have greatly increased our knowledge and understanding of PUI sources and their evolution. Within the past few years, two important sources of supra-thermal pick-up ions have been discovered, the inner and outer source, which appear to be related to interstellar and interplanetary dust particles.

6. New Missions

6.1. Novel Solar and Heliospheric Research with Solar Orbiter

Solar Orbiter (SO) is an ESA mission that will be launched into a heliocentric orbit in 2012. E. Marsch (Max-Planck-Institute for Aeronomy, Germany) described the scientific rationale for and the experimental approach to SO.

SO will carry out both in situ and remote measurements. It will measure in-situ the properties of fields and particles in the unexplored near-Sun heliosphere in three dimensions. It will remotely investigate fine-scale structures and events in the magnetically coupled layers of the Sun's atmosphere. During portions of the orbit, SO will effectively corotate with the Sun and identify through this corotation links between activity on the Sun's surface and the resulting evolution of the inner heliosphere. During the high latitude portions of its orbit, SO will observe the Sun's polar regions and the equatorial projection corona. Finally, the

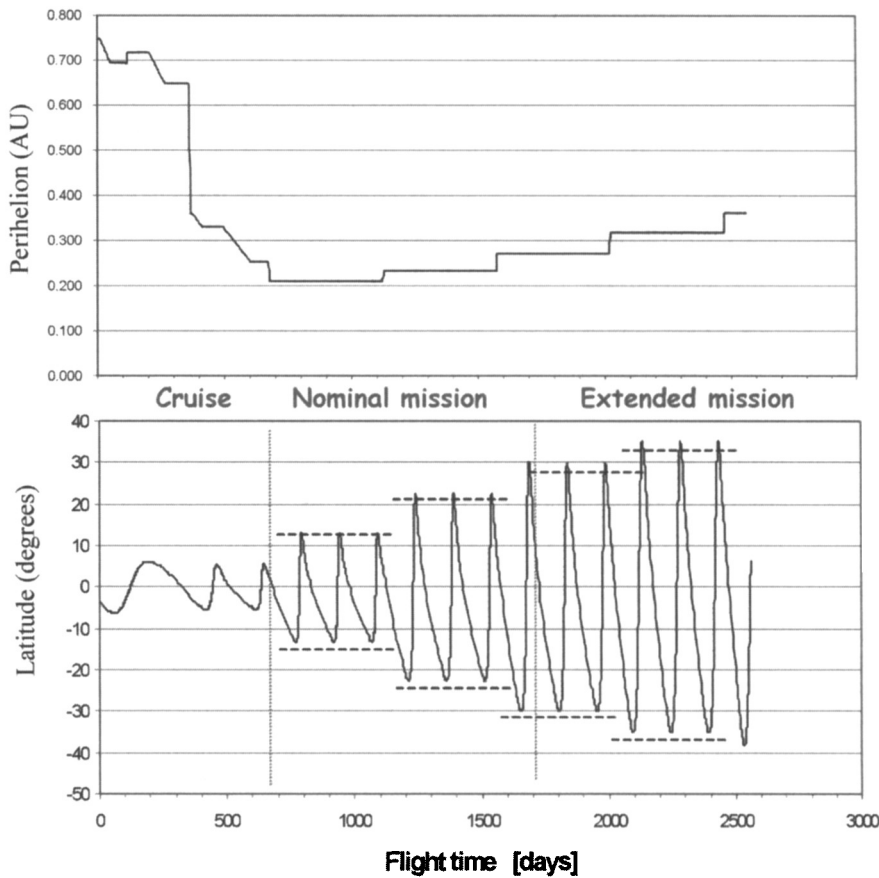


Figure 14. Perihelion distance and helio latitude achieved by the Solar Orbiter orbit over the lifetime of the mission, measured in days after launch.

unique virtue of the SO mission is that it will render possible the first close-up observations made from a near-Sun platform.

The experiment complement of SO is designed to fully exploit the heliospheric location of the platform. At closest approach (0.2 AU perihelion, Figure 14) to the Sun, optical observations with 35 km pixels at all wavelengths and radiance measurements resolving filling factors will be made. The out-of-ecliptic (up to 38° helio latitude) orbits will allow the magnetic field and magnetoconvection in the Sun's polar region to be observed directly and will provide synoptic views of the equatorial streamer belt. Corotation of the spacecraft with the Sun will enable us to disentangle spatial from temporal effects.

The fundamental questions addressed by the mission are: Why does the sun vary and how does the solar dynamo work? What are the fundamental processes at work in the solar atmosphere and heliosphere? What are the links between the magnetic field dominated regime in the solar corona and the particle regime in the heliosphere? Addressing these questions will further make SO a valuable

addition to the International Living With a Star Program that is discussed in §6.2.

6.2. The International Living With a Star Program

The International Living With a Star (ILWS) Program will provide an umbrella for forging international coordination, cooperation, and bi-lateral and multi-lateral agency collaborations in studies of: How and why does the Sun vary? How does the Earth respond (and vary)? What are the impacts on humanity? The mission statement is to “Stimulate, strengthen, and coordinate space research to understand the governing processes of the connected Sun-Earth system as an integrated entity.” This will be achieved through a systems approach that will quantify the physics, dynamics, and development of the Sun-Earth connected system through the entire range of conditions occurring in the 11 year solar cycle. To do this, it incorporates space missions, additional data sources, data dissemination, and supporting theory and modeling. Membership presently includes Canada, Europe, the USA, and Russia. R. Marsden (European Space Agency, Noordwijk, The Netherlands), in collaboration with H. Opgenoorth (European Space Agency, Noordwijk, The Netherlands) and L. Guhathakurta (NASA, USA), presented ILWS for this consortium.

ILWS expects to accomplish the following:

- Delineate key processes involved in the generation and propagation of solar and geomagnetic disturbances.
- Characterize & quantify the dynamics and evolution of the solar interior, surface, and corona.
- Characterize and quantify the dynamics of the Earth’s upper upper atmosphere and current systems, electric fields, and particle populations in the near-Earth space.
- Characterize and quantify global dynamics that cause enhanced magnetospheric radiation zones and satellites to transit these zones.

The missions included in ILWS are shown in Figure 15. These are selected on the basis of the systems approach, instrumentation, and ability to complement measurements made on other missions. The time line at the bottom shows the initiation of ILWS this year and its continuation past the middle of the next decade.

The ILWS mission fleet is a consequence of circumstances rather than planning. Therefore, there are obvious shortfalls. Specifically,

- There is insufficient spacecraft coverage to sample simultaneously all critical regions & phenomena of the complex, time-varying geo-space environment.
- Solar wind is to be sampled at only a few points.
- There is inadequate measurement of solar high energy phenomena (e.g. flares and energetic particles) currently planned for the next solar maximum.
- There is a gap in the measurement of solar irradiance.

ILWS will address these shortfalls in planning for the Solar Orbiter, Solar Sentinels, and long-range mission strategy. The planning will be designed to continually clarify opportunities and possibilities and incorporate community participation in ILWS planning and priority setting.

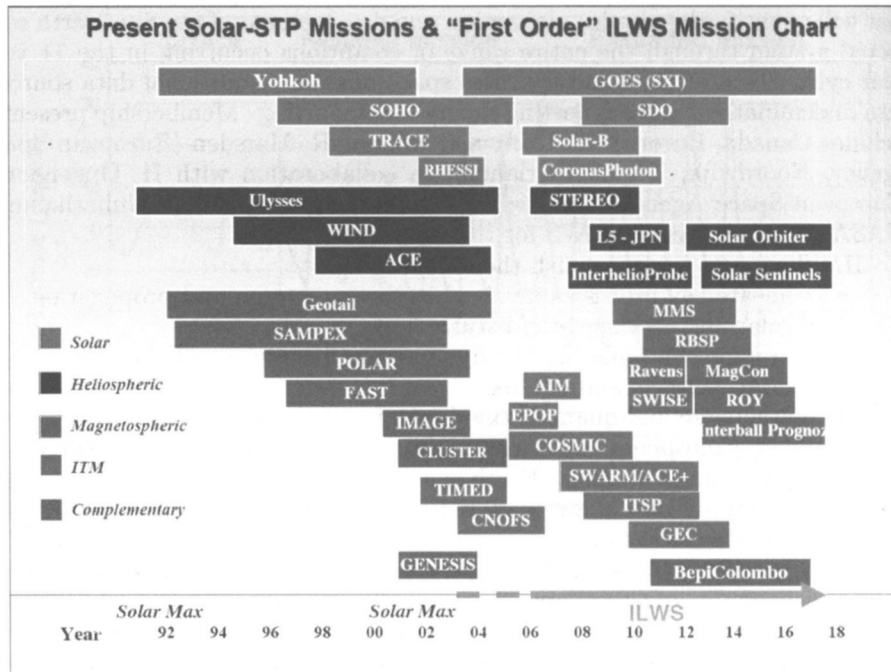


Figure 15. Chart showing existing, planned, and proposed missions that are part of the ILWS Mission.

7. Poster Papers

Title	Authors
Magnetic solar cycle related heliospheric density anomalies	S. Ananthakrishnan, P. Janardhan, V. Balasubramanian
The solar flare myth	H. V. Cane
Stereo observations of the Sun and interplanetary medium, space triangulation, and the problems of creation of the long-life solar stereoscopic observatory - Russia	V. M. Grigoriev, P. G. Papushev, S. A. Chuprakov, M. S. Chubey, G. I. Eroshkin, V. N. L'vov, and V. V. Pashkevich
Analysis of the Faraday rotation in the measurement of transverse magnetic field	J. Dun and H. Zhang
Tomography of heliospheric features developed for SMEI (<i>Invited</i>)	B. V. Jackson, P. P. Hick, and A. Buffington
Is the chromosphere heated by oscillations? (<i>Invited</i>)	W. Kalkofen
Type II bursts: dynamic spectra and source locations	S. A. Knock, I. H. Cairns, and P. A. Robinson
Radio emission from upstream of the Earth's bowshock	Z. Kuncic, I. H. Cairns, S. Knock, and P. A. Robinson
Nonlinear electrostatic decay of beam-driven Langmuir waves	B. Li, A. J. Willes, P. A. Robinson, and I. H. Cairns
Dynamics and entry of small dust grains near the heliosphere	I. Mann and A. Czechowski
Dynamic spectra for 2-3 kHz radio emission	J. Mitchell, I. Cairns, and P. A. Robinson
Regimes of stochastic wave growth in space plasmas	P. A. Robinson, B. Li, and I. Cairns
North-south offset of heliospheric current sheet and its causes	P. Zhao, J. T. Hoeksema, and P. Scherrer
First steps to solar feature catalogues	V. V. Zharkova

References

- Arge, C.N., & Mullan, D. J. 1998, Sol. Phys. 182, 293
 Bemporad, A., Poletto, G., Suess, S. T., Ko, Y. K., Parenti, S., Riley, P., Romoli, M., & Zurbuchen, T. 2003, ApJ, 593, 1146
 Brandt, P. C., Mitchell, D. G., Roelof, E. C., & Burch, J. L. 2001, Sol. Phys. 204, 377.
 Caligari, P., Moreno-Insertis, F., & Schussler, M. 1995, ApJ, 441, 886.
 Cairns, I. H., & Zank, G. P. 2002, GRL, 29(7), 47.
 Cranmer, S.R., et al. 1999, ApJ, 511, 481

- Demars, H., & Schunk, R. 1979, J. Phys. D, 12, 1051.
- Deng, Y., Wang, J., Yan, Y., Zhang, J. 2001, Sol. Phys., 204, 11
- Feldman, U., Schüle, U., Widing, K.G., & Laming, J.M. 1998, ApJ, 505, 999
- Fludra, A., & Schmelz, J.T. 1999, A&A, 348, 286
- Fisk, L. A. 1996, JGR, 101, 1011.
- Gaidos, E. J., Güdel, M., & Blake, G. A. 2000, GRL, 27, 501.
- Gudiksen, B. V. & Nordlund, Å 2002, ApJ, 572, 113.
- Gurnett, D. A., Kurth, W. S., Allendorf, S. C., & Poynter, R. L. 1993, Science, 262 (5131), 199.
- Hayashi, K., Kojima, M., Tokumaru, M., & Fujiki, K. 2003, JGR, 108,
- Hansteen, V., Leer, E., & Holzer, T.E. 1997, ApJ, 482, 498
- Heber, B. et al. 2003, Ann. Geophys. 21, 1275
- Henoux, J.-C., 1998, Space Sci. Rev., 85, 215
- Jackson, B. V., Hick, P., & Buffington, A. 2003, in SPIE Conf. Proc. 4853, ed. S. L. Keil & S. V. Avakya (Bellingham, WA: SPIE Press), 23.
- Izmodenov, V., Gloeckler, G., & Malama, Y. 2003, GRL, 30(7), 1351.
- Izmodenov, V., & Alexashov, D. 2003, Astr. Lett., 29, 58.
- Ko, Y.-K., Raymond, J., Li, J., Ciaravella, A., Michels, J., Fineschi, S., & Wu, R. 2002, ApJ, 578, 979
- Kojima, M., Fujiki, K., Ohmi, T., Tokumaru, M., Yokobe, A., & Hakamada, K. 2001, JGR, 106(A3), 15677, SSH2-1.
- Krivova, N. A., Solanki, S. K., Fligge, M., & Unruh, Y. C. 2003, A&A, 399, L1.
- Kurth, W. S., & Gurnett, D. A. 2003, JGR, 108(A10), LIS 2-1.
- Laming, J.M., & Feldman, U. 2003, ApJ, 591, 1257
- Lanzerotti, L. J., Meford, L. V., MacLennan, C. G., Kraus, J. S., Kappenman, J., & Radasky, W. 2001, Sol. Phys., 204, 351.
- Lanzerotti, L. J., & Sanderson, T. 2001, in The Heliosphere Near Solar Minimum: The Ulysses Perspective, ed. A. Balogh, R. G. Marsden, & E. J. Smith (Chichester, UK: Praxis Publishing), 259.
- Lenz, D., Lou, Y.-Q., & Rosner, R. 1998, ApJ, 504, 1020
- Liu, R-Y., Hu, H-Q., Xu, Z-H., Sato, N., & Fraser, B. J. 2001, Sol. Phys., 204, 307.
- Lie-Svendsen, O., Hansteen, V. H. & Leer, E. 2002, JGR, 107(A10), SSH18-1.
- Lie-Svendsen, O., Hansteen, V. H., Leer, E. & Holzer, T. E. 2002, ApJ 566, 562.
- Marsch, E. 1991, in Physics of the Inner Heliosphere vol. 2 ed. R. Schwenn & E. Marsch (Heidelberg: Springer-Verlag), 159.
- McComas, D. J., Elliott, H. A., Schwadron, N. A., Gosling, J. T., Skoug, R. M., & Goldstein, B. E. 2003, GRL, 30, 24.
- Neugebauer, M., Forsyth, R. J., Galvin, A. B. et al. 1998, JGR, 103, 14587.
- Nolte, J. T., Krieger, A. S., Timothy, A. F., et al. 1976, Sol. Phys. 46, 303.
- Ohmi, T., Kojima, M., Yokobe, A., Tokumaru, M., Fujiki, K., & Hakamada, K. 2001, JGR, 106, 24923.
- Ohmi, T., Kojima, M., Fujiki, K., Tokumaru, M., Hayashi, K., & Hakamada, K. 2003, GRL, 30, 62.
- Peter, H. 1998, A& A, 335, 691
- Phillips, K. J. H., Sylwester, J., Sylwester, B., & Landi, E. 2003, ApJL 589, 113
- Raymond, J.C., et al. 1997, Sol. Phys., 175, 645
- Reiner, M. J., Kaiser, M. L., Karlický, M., Jiřička, K. & Bougeret, J.-L. 2001, Sol. Phys., 204, 123

- Smith, E. J., et al., 2003, GRL, 30, 19
- Solanki, S. K., & Krivova, N. A. 2003, JGR, 108, SSH7-1.
- Turcotte, S. & Wimmer-Schweingruber, R. F. 2002, JGR, 107, SSH5-1
- Vögler, A. & Schüssler, M. 2003, AN, 324, 399
- Wang, C., Richardson, J. D., & Burlaga, L. 2001, Sol. Phys., 204, 413
- Wang, Y.-M. & Sheeley, N. R. 1990, ApJ, 355, 726.
- Whang, Y. C., Burlaga, L. F., Ness, N. F., & Smith, C. W. 2001, Sol. Phys., 204, 253
- Widing, K. G., & Feldman, U. 2001, ApJ, 555, 426
- Wimmer-Schweingruber, R. F. & Bochsler, P. 2001, AIP Conf. Proc. 598, 399
- Wimmer-Schweingruber, R. F. & Bochsler, P. 2003, GRL, 30, 49
- Wood, B. E., Müller, H.-R., & Zank, G. P. 2000, ApJ, 542, 493.
- Yan, Y., Aschwanden, M. J., Wang, S., & Deng, Y. 2001, Sol. Phys., 204, 27
- Zhang, J., Wang, J., Deng, Y., & Wu, D. 2001, ApJ, 548, L99.